

1 **Future Directions for Whole Atmosphere Modelling: Developments in the**
2 **context of space weather**

3
4 **David R. Jackson¹, Tim J. Fuller-Rowell², Dan J. Griffin¹, Matthew J. Griffith³,**
5 **Christopher W. Kelly⁴, Daniel R. Marsh^{4,5} and Maria-Theresia Walach⁶**

6 ¹Met Office, Exeter, UK

7 ²University of Colorado, USA

8 ³University of Bath, UK

9 ⁴University of Leeds, UK

10 ⁵National Center for Atmospheric Research, USA

11 ⁶Lancaster University, UK

12 Corresponding author: David Jackson (david.jackson@metoffice.gov.uk)

13 **Key Points:**

- 14 • We have reached a paradigm shift, where any self-respecting space weather model of the
15 upper atmosphere now needs to have some representation of the lower atmosphere.
- 16 • Further model developments are required in several key areas, including dynamical cores
17 and the improved representation of gravity waves.
- 18 • A roadmap of future actions is presented to ensure good progress continues to be made.
19 This includes the development of a multi-model verification strategy.
20

21 **Abstract**

22 Coupled Sun-to-Earth models represent a key part of the future development of space weather
23 forecasting. With respect to predicting the state of the thermosphere and ionosphere, there has
24 been a recent paradigm shift; it is now clear that any self-respecting model of this region needs to
25 include some representation of forcing from the lower atmosphere, as well as solar and
26 geomagnetic forcing. Here we assess existing modeling capability and set out a roadmap for the
27 important next steps needed to ensure further advances. These steps include a model verification
28 strategy, analysis of the impact of non-hydrostatic dynamical cores, and a cost-benefit analysis of
29 model chemistry for weather and climate applications.

30 **Plain Language Summary**

31 Numerical models that comprehensively simulate the region between the Sun and the Earth
32 represent a key part of the future development of space weather forecasting. With respect to
33 predicting the Earth's upper atmosphere, there has been a recent paradigm shift; it is now clear
34 that any self-respecting model of this region needs to include some representation of impacts
35 from below (the lower atmosphere) as well as from above (solar variability and the effects of
36 solar wind fluctuations). Here we assess existing modeling capability and set out a roadmap for
37 the important next steps needed to ensure further advances. These steps include a strategy for
38 checking the accuracy of the models, an analysis of the impact of methods chosen to represent
39 upper atmosphere dynamics, and an assessment of the relative benefits of comprehensive (but
40 expensive) and simplified (but inexpensive) model representations of upper atmosphere
41 chemistry.

42

43 **1. Introduction**

44

45 We are at the stage in the development of operational space weather forecasts where individual
46 models of components of the Sun-to-Earth domain (including the ionosphere and the
47 thermosphere) are beginning to be coupled together. Such a coupled modelling system,
48 constrained by assimilation of near real time observations, has the potential to provide
49 considerably better forecasts than currently available. It is clear that representing the impact of,
50 for example, a Coronal Mass Ejection, across the whole Sun-to-Earth domain can potentially
51 improve forecasts in the ionosphere. The potential for improved forecasts has already been
52 demonstrated for parts of the Sun to Earth system. For example, coupling a global
53 magnetosphere model with an inner magnetosphere drift physics model considerably improves
54 forecasts of geomagnetic storms (Liemohn et al., 2018), and improved representation of the
55 thermosphere leads to improved ionospheric evolution (e.g. Chartier et al., 2013). In addition,
56 there is a strong connection between the lower atmosphere state and the ionosphere that was
57 highlighted initially by Immel et al. (2006) and demonstrated in later modelling studies (eg
58 Pedatella et al., 2016). Furthermore, data assimilation schemes are already used for operational
59 ionosphere models (e.g. Schunk et al., 2016) and experimental systems show that assimilation
60 can improve model initial conditions in the thermosphere (e.g. Murray et al., 2015), the
61 magnetosphere (e.g. Merkin et al., 2016) and the heliosphere (e.g. Lang et al., 2019).

62

63 However, it is also becoming increasingly apparent that, in addition to correctly specifying this
64 space weather forcing, thermosphere and ionosphere forecasts can also benefit from an accurate

65 representation of coupling from within and below. The motivation for a whole atmosphere model
 66 (i.e., a model that extends from the ground up to the exobase) is thus two-fold:

67

- 68 • Recent research (e.g., Chartier et al., 2013, 2016, Hsu et al., 2014) has shown that, no
 69 matter how accurately one represents the current ionospheric state, the quality of the
 70 subsequent ionospheric forecasts crucially depends on the ability to also represent the
 71 thermosphere and its evolution.
- 72 • Both the ionosphere and thermosphere are sensitive to forcing from the lower
 73 atmosphere. The seminal paper by Immel et al. (2006) indicated connections between
 74 tidal patterns in the lower thermosphere and the F-region ionosphere, and noted that the
 75 tidal structure was linked to patterns of convection in the equatorial troposphere.
 76 Furthermore, numerous papers (e.g. Liu and Roble, 2002, Goncharenko et al., 2010a,
 77 2010b, McDonald et al., 2018, Pedatella et al., 2012) have shown how planetary wave
 78 forcing, specifically via stratospheric sudden warmings (SSWs), can affect lower
 79 thermospheric tides and thus the ionosphere.

80

81 Akmaev (2011) reviewed whole atmosphere models at a time when these models were quite new
 82 and our understanding of the links between the lower and upper atmosphere was developing. A
 83 Whole Atmosphere Modelling Workshop was held in Tres Cantos, Spain in June 2018 and a
 84 strong consensus emerged: the need to have some representation of the lower atmosphere in
 85 space weather models of the upper atmosphere. This is highly significant for the continued
 86 development of whole atmosphere models. In this commentary we review existing models, how
 87 their building blocks can be further developed, and how we can use observations (via data
 88 assimilation and verification) to confront the model simulations and potentially produce
 89 improved forecasts.

90

91 2. Existing Models

92

93 There are three current whole atmosphere space weather models:

94

- 95 • The Whole Atmosphere Model (WAM) (Akmaev et al., 2008, Fuller-Rowell et al., 2008)
 96 is based on the US National Weather Service Numerical Weather prediction model and
 97 extends from the surface to around 600 km. It is being combined with a separate
 98 ionosphere model Ionosphere Plasmasphere Electrodynamics (IPE; Maruyama et al.,
 99 2015) to produce a coupled model of the ionosphere and neutral atmosphere. WAM
 100 represents both the mean state and tides in the thermosphere well (e.g Lieberman et al.,
 101 2013 show good agreement with diurnal and time mean Challenging Mini Satellite
 102 Payload (CHAMP) winds). The pattern of changes seen in ionospheric vertical plasma
 103 drift and Total Electron Content (TEC) (that occur in response to SSW forcing from
 104 below) agrees well with observations (e.g. Wang et al., 2014).
- 105 • The Whole Atmosphere Community Climate Model with thermosphere and ionosphere
 106 extension (WACCM-X (Liu et al., 2010, Liu et al., 2018) is focused primarily on **climate**
 107 timescales (in contrast to WAM, which is focused on **weather** forecast timescales). With
 108

109 a comparable altitude range to WAM, it has a much more detailed representation of
 110 neutral and ion chemistry. Liu et al (2018) report that in WACCM-X the amplitudes and
 111 seasonal variations of atmospheric tides in the mesosphere and lower thermosphere
 112 (MLT), equatorial ionosphere anomaly structures and storm-time ionospheric behavior
 113 are all in good agreement with observations.

- 114
- 115 • The Ground to topside model of the Atmosphere and Ionosphere for Aeronomy (GAIA)
 116 combines neutral atmosphere, ionospheric and electrodynamic models. The neutral model
 117 covers the entire atmosphere from the Earth's surface up to the top of the thermosphere
 118 and contains a comprehensive range of physical parametrizations (e.g. Fujiwara and
 119 Miyoshi, 2010). Jin et al. (2012) show the ability of GAIA to model the impact of an
 120 SSW on migrating tides and the associated ionospheric response, with in general good
 121 agreement shown with Sounding of the Atmosphere using Broadband Emission (SABER)
 122 and Constellation Observing System for Meteorology, Ionosphere, and Climate
 123 (COSMIC) observations.
 124

125 [For clarification: **weather** models focus on short forecast timescales (often less than 10 days),
 126 and use as fine a resolution as possible in order to represent meteorological features such as
 127 weather fronts. Since forecast quality will depend on initial conditions, weather models must be
 128 initialized using data assimilation. Coupling to other models (such as an ocean model) is usually
 129 not required on forecast timescales, and the need to run quickly in near real time precludes the
 130 use of such coupled models and it is necessary to use fast, less complex representations of
 131 physics and chemistry. **Climate** models are run for long forecast timescales such as annual or
 132 multi-decadal periods, and so generally have coarser resolutions than weather models. Coupling
 133 to comprehensive models of the Earth system (chiefly ocean and atmospheric chemistry models)
 134 is required to represent long term variability and climate change. For the specific case of whole
 135 atmosphere models, WAM and WACCM do not completely meet the description given above
 136 (for example, WACCM can run at a finer horizontal resolution than WAM), but the WAM
 137 chemistry scheme is simple and designed for fast weather forecasts, whereas the WACCM
 138 chemistry scheme is considerably more complex, and it can be coupled to an ocean model. This
 139 enables WACCM to be used in activities like the Coupled Model Intercomparison Project 5
 140 (CMIP5), studying, for example, climate change from 1850 (Marsh et al., 2013) and climate
 141 impacts associated with long term ozone change (Eyring et al., 2013).]
 142

143 **3 Building Blocks for better models**

145 **3.1 Dynamics – gravity waves and dynamical formulation**

146

147 The representation of gravity waves is very important for accurate modelling of the
 148 thermosphere. They are the prime driver of the middle atmosphere circulation and affect tidal
 149 amplitudes, and thus can influence the mechanisms connecting the lower atmosphere with the
 150 thermosphere and ionosphere (see e.g. Yiğit et al., 2016). Furthermore, accurate simulation of
 151 medium and small-scale travelling ionospheric disturbances (MSTIDs), and associated
 152 ionospheric plasma bubbles which impact precision application of Global Navigation Satellite

153 System (GNSS) data, require the ability to represent sub grid-scale gravity waves in whole
154 atmosphere models. This information on MSTIDs could be input into existing tools for
155 estimating GNSS positioning error from TIDs (e.g. Lejeune et al., 2012). Gravity waves also
156 play an important role in the transport of chemical constituents, which is discussed in more detail
157 later.

158 Liu et al. (2014) ran a fine resolution ($0.25^\circ \times 0.25^\circ$ horizontal, 0.1 scale height vertical) version
159 of WACCM to demonstrate the simulation and impact of gravity waves up to around 100 km.
160 However, it is not clear whether such resolutions are needed at higher levels in the thermosphere.
161 Miyoshi et al. (2018) showed that a GAIA simulation with a resolution of $1^\circ \times 1^\circ$ produces
162 fluctuations in electron density with length scales less than around 1000 km and periods of less
163 than around 2 hours, which are in good agreement with observations and which are not seen in a
164 coarser resolution ($2.5^\circ \times 2.5^\circ$) simulation. The fluctuations reported by Miyoshi et al. are
165 attributed to TIDs that are excited by secondary gravity waves. These waves typically have
166 horizontal wavelengths of around 100 km to several 1000s of km (Vadas and Crowley, 2010).
167 This also appears consistent with Gardner and Schunk (2011), who indicated observed gravity
168 waves in the thermosphere typically have horizontal scales of around 100-500 km. Furthermore,
169 at altitudes above around 110 km molecular viscosity and thermal conduction strongly influence
170 gravity wave filtering and dissipation, as opposed to winds and wave breaking lower in the
171 atmosphere (see e.g. Vadas and Fritts, 2005). Accordingly, lower atmosphere gravity wave
172 parametrization schemes may not be appropriate in the thermosphere. Schemes that specifically
173 focus on parameterizing gravity waves in the thermosphere (e.g. Yiğit et al., 2008) could be
174 adopted for coarse horizontal resolution whole atmosphere model simulations.

175 Presently, WAM, WACCM-X and GAIA use hydrostatic dynamical cores. The dynamical core
176 solves the governing fluid and thermodynamic equations in the model on resolved scales, while
177 parametrizations represent sub-grid-scale processes and other processes not included in the
178 dynamical core such as radiative transfer (Thuburn, 2008). Certainly for some applications, such
179 as satellite drag, the hydrostatic approximation appears adequate (see e.g. Bruinsma et al., 2018),
180 but there is still a need to identify the impact on model results that may arise from non-
181 hydrostatic processes. For some applications that require accurate representation of the wave
182 fluctuations (such as radio wave propagation in the bottom-side F region for HF applications),
183 the hydrostatic approximation may be inappropriate in the thermosphere, and adoption of non-
184 hydrostatic (non-H) dynamical cores appears to be a logical next step. The hydrostatic
185 approximation breaks in the presence of large vertical accelerations (e.g. Curry and Webster,
186 1998), and using a non-H dynamical core may affect the modelled gravity wave spectrum,
187 particularly when applied at fine horizontal resolution. High frequency waves with horizontal
188 wavelength less than $4\pi H$ (where H is scale height) should be treated non-hydrostatically
189 (Akmaev, 2011). For example, Eckermann et al. (2016) showed observations of gravity waves
190 that had propagated from the surface to the lower thermosphere with vertical velocities of several
191 tens of ms^{-1} . They concluded that these waves must be non-hydrostatic, since if they were
192 hydrostatic they would have broken in the troposphere or lower stratosphere rather than
193 propagating higher. Therefore, selection of a non-H dynamical core can affect the modelled
194 gravity wave spectrum in the MLT, and thus the simulation of MSTIDs. A fine horizontal
195 resolution is required to represent such waves in the first place, and, given that whole atmosphere
196 models currently have resolutions of ~ 100 km to 200 km, the case for using non-H cores at such

197 resolutions is not yet well made. Three new whole atmosphere models are being developed
198 which use non-H cores: the Navy Global Environmental Model (NAVEM; e.g. McCormack et
199 al., 2017), the Met Office Extended Unified Model (UM) and WAM, where the current
200 dynamical core is being replaced with the Geophysics Fluid Dynamics Laboratory Finite-
201 Volume on a Cubed-Sphere (FV3) non-H core (Ullrich et al., 2017). In addition, Borchert et al.
202 (2018) report on work to extend the ICOSahedral Non-hydrostatic (ICON) general circulation
203 model up to 150 km altitude. NAVEM and the UM have the option to switch between
204 hydrostatic and non-H formulations, and both these models could play key roles in evaluating the
205 importance of non-H cores in whole atmospheric models.

206 There can also be issues with the robustness of non-H dynamical cores in the thermosphere.
207 Griffin and Thuburn (2018) showed that the UM required the addition of molecular viscosity and
208 diffusion in order to realistically stabilize artificial wave growth, as this viscosity has a
209 significant damping effect in the thermosphere. Another challenge arises above the turbopause
210 (around 105 km) where diffusive separation means that air parcels are no longer turbulently
211 mixed and the molecular weight of a species determines its dynamical evolution. Therefore,
212 ideally each species should have its own set of dynamical equations that need to be solved. The
213 molecular diffusion is also affected by variable gravity which in turn modifies atmospheric scale
214 heights. Thus, there is a need to reformulate the dynamical core to properly model the individual
215 species, as well as a need to add a correction to the thermal equation.

216

217 **3.2 Radiation and chemistry**

218

219 Accurate radiation and chemistry schemes are needed throughout the whole atmosphere model
220 domain, most obviously in the MLT where the radiation scheme calculates the absorption of
221 solar radiation that drive the large rise in temperature with height there. This means that
222 radiation schemes need to include the far ultraviolet (FUV), extreme ultraviolet (EUV) and soft
223 x-ray spectral ranges that are usually ignored in lower atmosphere models. In the MLT, heating
224 from exothermic reactions becomes important (especially during polar night) and must be
225 accounted for to correctly simulate the thermal structure. Quenching of $O(^1D)$ is a large source of
226 heating throughout the MLT, above 100 km ion reactions and reactions involving atomic
227 nitrogen are significant sources of heat, and below 100 km O_x and HO_x reactions are the
228 dominant producers of chemical heating (Marsh et al., 2007). In addition, above the mid-
229 mesosphere, local thermodynamic equilibrium (LTE) schemes need to be replaced by non-LTE
230 formulations, since both Near Infrared heating and Infrared cooling are over-estimated by the
231 LTE schemes. The Fomichev non-LTE parametrization (Fomichev et al., 2005, 2008; Ogibalov
232 and Fomichev, 2003), is the only scheme currently available for Earth GCMs. Its formulation is
233 based on recent atmospheric conditions and it lacks the adaptability to be used for climate
234 change experiments. The UM's radiation scheme is being extended to include FUV and EUV
235 wavelengths. The scheme is highly flexible, with the option of being run using different spectral
236 resolutions. In future it could be further modified to include a more comprehensive
237 representation of non-LTE heating, possibly based on a scheme developed for Mars (López-
238 Valverde and López-Puertas, 1994), which potentially represents a considerable improvement on
239 the Fomichev scheme. Since the scheme is also publically available it could be a highly
240 important community resource for future collaborative whole atmosphere model development.

241

242 While only relatively few major chemical reactions are sufficient to adequately represent the
243 large rise in temperature in the MLT (Marsh et al., 2007), other challenges remain. Below 85 km
244 the atmospheric chemistry is dominated by compounds, and above 100 km by ion chemistry.
245 Particularly interesting chemistry exists in between, where atoms including highly reactive
246 hydrogen and oxygen atoms are in abundance, with maximum mixing ratios observed at around
247 85 km and 90-95 km, respectively (Plane et al., 2015). WACCM simulations of metal layers
248 originating from the ablation of meteoroids in the MLT give good model agreement with data at
249 mid latitudes, but show worse agreement at high latitudes. For example, for Fe chemistry Feng et
250 al. (2013) shows that the model significantly overestimates winter Fe and underestimates
251 summer Fe compared to observations from three Antarctic ground-based lidars. This implies that
252 the model vertical transport of chemical species may be significantly underestimated. A possible
253 issue is that global models cannot capture transport associated with small scale gravity waves,
254 and adding diffusion terms to account for this does help with reducing the large bias.
255 Observations of MLT chemistry are sparse, and thus there is great scope for new observations to
256 significantly improve our knowledge of the interaction between chemistry and transport. For
257 example, recent observations made by the Atmospheric Chemistry Experiment (ACE) indicate
258 nitrous oxide (N_2O) is being produced in the MLT (Sheese et al., 2016). N_2O is a precursor of
259 odd nitrogen (NO_x) which destroys stratospheric ozone. A new chemical source of N_2O has been
260 successfully added to WACCM by Kelly et al. (2018). Model simulations were able to capture
261 the observed N_2O layer and well replicate seasonal variations near the poles. Recent studies have
262 also highlighted the importance of radiation and chemistry schemes working together to produce
263 the strong NO cooling which is observed in the immediate aftermath of geomagnetic storm-time
264 thermospheric heating (e.g. Knipp et al., 2017) .

265 **3.3 Ionosphere and electrodynamics**

266
267 The coupling between the thermosphere and ionosphere is important, as mentioned above, in
268 ensuring a more accurate evolution of the ionospheric state. Fang et al. (2013) performed an
269 intercomparison of a range of ionospheric models. It is clear that the thermosphere / ionosphere
270 coupling was modelled better when the models employed a fully consistent representation of the
271 electrodynamics. This led to the development of the IPE model, which includes the following
272 requirements: it represents the ionosphere globally with similar resolution to the neutral
273 atmospheric model (WAM) it is coupled to; it uses self-consistent electrodynamics for quiet and
274 storm-time dynamo processes; it uses a coupling infrastructure.

275
276 Also important is an accurate representation of the electric field and its variation. There are
277 limitations with current empirical electric field models, such as those developed by Heelis (1982)
278 and Weimer (2005). These are climatological in nature, but more observations are required to
279 capture the electric field variability. The introduction of Super Dual Auroral Radar Network
280 (SuperDARN) data crucially adds extra observations polewards of 40° geomagnetic latitude (as
281 well as providing observations at lower latitudes), and the deviation of SuperDARN high latitude
282 electric fields from the average ionospheric state shows the importance of accounting for the
283 prior evolution of the ionospheric state. M.-T. Walach (presentation available at
284 [http://www.research.lancs.ac.uk/portal/en/activities/characterising-and-understanding-temporal-variability-in-ionospheric-flows-using-superdarn-data\(21f8f287-e085-4418-8a1c-387d597ef2f0\).html](http://www.research.lancs.ac.uk/portal/en/activities/characterising-and-understanding-temporal-variability-in-ionospheric-flows-using-superdarn-data(21f8f287-e085-4418-8a1c-387d597ef2f0).html)) used SuperDARN data to show that greater solar wind corresponds to
285 greater variability in convection, and is currently investigating the drivers of this variability in
286
287

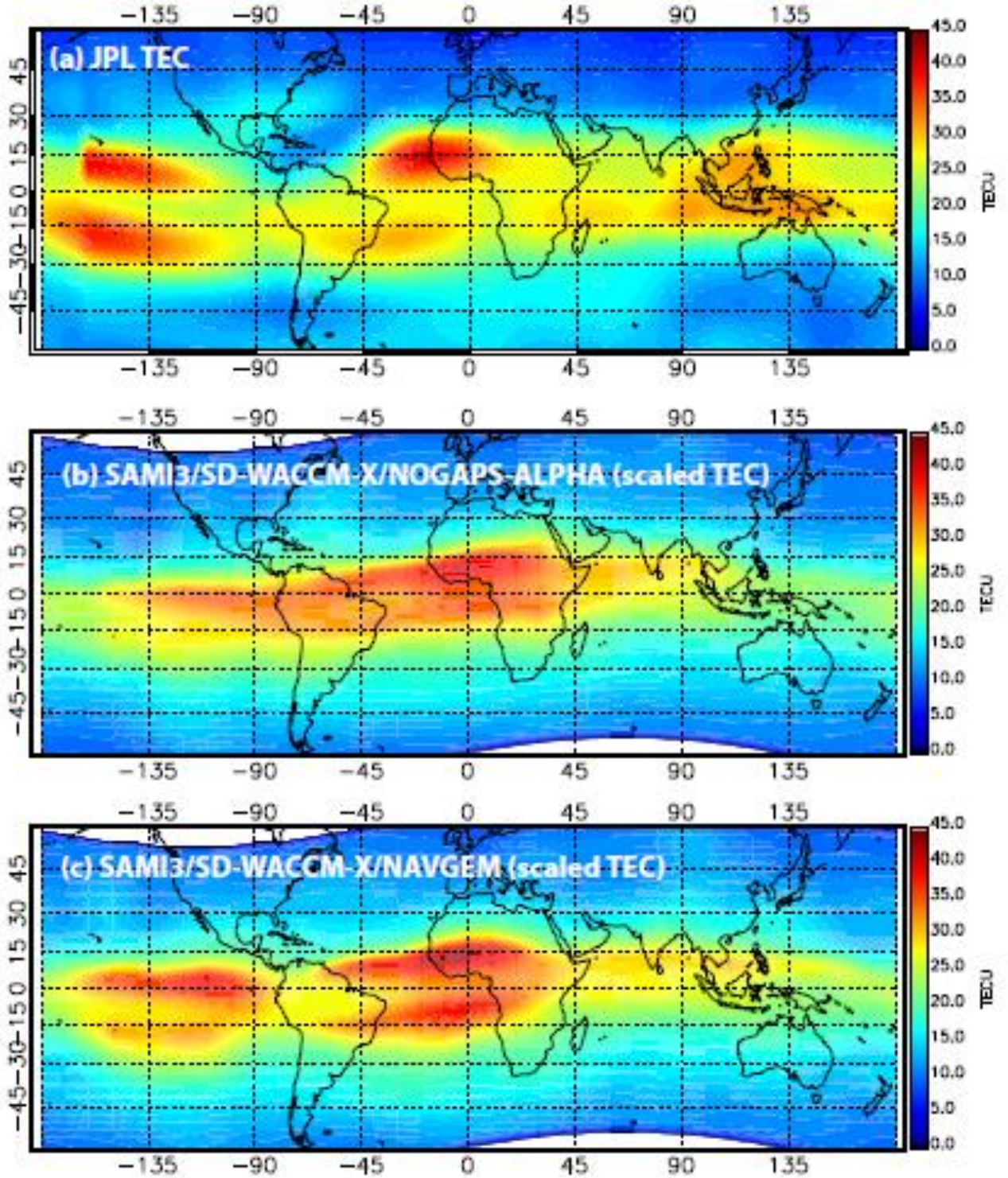
288 more detail. Use of SuperDARN observations in the Canadian Ionosphere and Atmosphere
289 Model (Martynenko et al., 2014) allows detailed features in the plasma density distribution to be
290 reproduced, especially in the topside ionosphere at high latitudes. Data from the Assimilative
291 Mapping of Ionospheric Electrodynamics (AMIE) can be used to assimilate multiple data
292 sources (SuperDARN) for testing in whole atmosphere models. The electric field model chosen
293 also influences modelled Joule heating, and it is important to continue to confront empirical
294 model-based estimates with observations (e.g., Billett et al., 2018).

295

296 **3.4 Observations for Data Assimilation and model verification**

297

298 Data Assimilation (DA) is important in attempting to ensure the model state is constrained to be
299 close to the true atmospheric state, and has been applied extensively in WACCM-X, WAM and
300 NAVGEM. DA in WACCM-X is done using an ensemble Kalman filter while the NAVGEM
301 DA system is a hybrid of 4D-Var and an ensemble Kalman Filter. The ensemble Kalman Filter
302 (Evensen, 1994) is a combination of a Kalman Filter (which evolves the state and estimate
303 covariance as new observations arrive) and Monte Carlo estimation methods (the full estimate
304 covariance matrix is explicitly evolved using an ensemble (sample of evolved states)). The
305 NAVGEM system has been shown to add a lot of value in the thermosphere. As an example, in
306 Figure 1 the observed wavenumber 4 structure in TEC is best reproduced when the NAVGEM
307 model thermosphere is forced by 3-hourly analyses; forcing by 6-hourly analyses is less
308 accurate. A major challenge is that the models cover a large altitude range, so waves can grow
309 exponentially, and to maintain model stability with DA, more damping is often added to deal
310 with spurious small scale waves. A consequence of this approach is that while model dynamics
311 and chemical transport are improved it is at the cost of the tidal amplitudes being too weak. To
312 add to the challenge in the upper atmosphere, data are sparse and processes act on shorter time
313 scales than in the lower atmosphere. Provision of considerably more near real time observations
314 of the upper atmosphere, particularly of the thermosphere, is vital if we are to exploit DA in
315 order to produce improved model forecasts.



316

317

Figure 1.

318 (a) JPL global ionospheric map of TEC on 12 January 2010 shown at constant local time of
 319 13:00 LT. (b) /NOGAPS-ALPHA simulation of TEC. (c) NAVGEN simulation of TEC. The
 320 simulated TEC is scaled by a factor of 0.7 (from McDonald et al., 2018)

321
322 To compound the lack of observations, the instruments that produce many of the upper
323 atmosphere observations used in the DA schemes (e.g. SABER, and MLS, the Microwave Limb
324 Sounder) are well past their nominal mission lifetimes and no follow-on programmes are
325 planned. Furthermore, these instruments only observe up to the lower thermosphere and
326 observations higher in the thermosphere are extremely sparse. The QB50 Cubesat project (e.g
327 Gill et al., 2013) focused on the building and launching of instruments to measure thermospheric
328 neutral density, but with little or no attention given to coordination and reception of data.
329 However the constellation of Cubesats used could be a pathfinder for a future operational
330 observations system, with the critical proviso that this constellation would need to be
331 underpinned by associated systems for near real time data reception and cross-calibration of data.
332 In addition, new data from the Global-scale Observations of the Limb and Disk (GOLD) mission
333 will help address the paucity of thermospheric data. The planned assimilation of GOLD O/N2
334 observations into WAM could test the assumption that temperature is a key variable for the
335 initialization of upper atmosphere models. Since O/N2 plays a key role as a diagnostic of
336 thermospheric transport, it is possible that future DA schemes could instead use O/N2 as a
337 primary control variable.

338
339 Model verification using existing data has proved invaluable. However, there is a need for a
340 consistent model verification strategy, and in particular community-wide agreement on which
341 metrics to compare – this could include basic seasonal variability, tide amplitudes and
342 variability, total electron content and the magnitude of the solar semidiurnal migrating tide. An
343 important consideration is to understand which observations are trusted and therefore should be
344 used to validate model output, and there are benefits in an Intergovernmental Panel on Climate
345 Change (IPCC) style model intercomparison, and a cooperative approach. An example is CMIP5
346 (Taylor et al., 2012) , in which an agreed set of experiments addressing major gaps in
347 understanding was run using multiple models, and output data were formatted in a common way
348 and made freely available via data portals. Empirical models may not be ideal for use as a level
349 of comparison and we suggest the employment of a more general model comparison system, e.g.,
350 as implemented in the International Land Model Benchmarking Project (ILAMB, Collier et al.,
351 2018).

352

353 **4. Future research directions and activities**

354

355 Based on the discussions throughout the workshop, the following roadmap for future
356 collaboration was agreed:

357

- 358 • Compare existing hydrostatic models to understand impacts of dynamical formulation
359 (also interactions with chemistry, the ionosphere, and radiation)
- 360 • Comparison of non-H and hydrostatic dynamical cores to assess impact of non-H cores
361 (and whether non-H is even needed at coarser resolution)
- 362 • Assess numerical cost / benefit of comprehensive chemistry schemes designed for
363 climate applications (e.g. WACCM) against simpler schemes designed for near-real time
364 operational use (e.g. as used in WAM)

- 365 • Development of a verification strategy and methodology which is required to underpin
 366 the above three actions. Clearly, it makes sense to make links with other activities to
 367 guide our future actions. These include the Committee on Space Research International
 368 Space Weather Action Team and the Community Coordinated Modeling Center (CCMC)
 369 Space Weather Modeling Capabilities Assessment (Scherliess et al., 2019)).

370 Of course, other issues that were discussed at the workshop (such as near real time availability of
 371 observations and DA) are very important, but the first focus here is on assessment and
 372 developing the whole atmosphere models themselves.
 373

374 There was a further suggestion that the joint development of parametrizations would be
 375 incredibly useful in unifying parametrization strategy across multiple models. The International
 376 Space Science Institute has a good setup for accomplishing verification with data, and this
 377 setting would be helpful for deciding a verification strategy. To monitor progress, it was also
 378 agreed to organize a follow up workshop in mid 2020.

379

380 **Acknowledgements**

381

382 We thank Fabrizio Sassi (Naval Research Laboratory) for supplying Figure 1. No data were
 383 generated for use in this manuscript.
 384

385 **References**

386

387 Akmaev, R. A., Fuller-Rowell, T. J., Wu, F., Forbes, J. M., Zhang, X., Anghel, A. F., et al.
 388 (2008). Tidal variability in the lower thermosphere: Comparison of Whole Atmosphere Model
 389 (WAM) simulations with observations from TIMED, *Geophys. Res. Lett.*, *35*, L03810.
 390 <https://doi.org/10.1029/2007GL032584>

391

392 Akmaev, R. A. (2011). Whole atmosphere modeling: Connecting terrestrial and space weather.
 393 *Reviews of Geophysics*, *49*, RG4004. <https://doi.org/10.1029/2011RG000364>

394

395 Billett, D. D., Grocott, A., Wild, J. A., Walach, M.-T., & Kosch, M. J. (2018). Diurnal variations
 396 in global Joule heating morphology and magnitude due to neutral winds. *Journal of Geophysical*
 397 *Research: Space Physics*, *123*, 2398–2411. <https://doi.org/10.1002/2017JA025141>

398

399 Borchert, S., Zhou, G., Baldauf, M., Schmidt, H., Zängl, G., & Reinert, D. (2018). The upper-
 400 atmosphere extension of the ICON general circulation model. *Geosci. Model Dev. Discuss.*
 401 <https://doi.org/10.5194/gmd-2018-289>

402

403 Bruinsma, S., Sutton, E., Solomon, S. C., Fuller-Rowell, T., & Fedrizzi, M. (2018). Space
 404 weather modeling capabilities assessment: Neutral density for orbit determination at low Earth
 405 orbit. *Space Weather*, *16*, 1806–1816. <https://doi.org/10.1029/2018SW002027>

406

407 Chartier, A. T., Jackson, D. R., & Mitchell, C. N. (2013). A comparison of the effects of
 408 initializing different thermosphere-ionosphere model fields on storm time plasma density
 409 forecasts. *J. Geophys. Res.*, *118*, 7329–7337. <https://doi.org/10.1002/2013JA019034>

- 410
411 Chartier, A. T., Matsuo, T., Anderson, J. L., Collins, N., Hoar, T. J., Lu, G., et al. (2016).
412 Ionospheric data assimilation and forecasting during storms, *J. Geophys. Res. Space Physics*,
413 *121*, 764–778. <https://doi.org/10.1002/2014JA020799>
414
- 415 Collier, N., Hoffman, F. M., Lawrence, D. M., Keppel-Aleks, G., Koven, C. D., Riley, W. J. et
416 al. (2018). The International Land Model Benchmarking (ILAMB) system: Design, theory, and
417 implementation. *J. Adv. Model. Earth Syst.*, *10*, 2731–2754.
418 <https://doi.org/10.1029/2018MS001354>
419
- 420 Curry, J. A., & Webster, P. J. (1998). Thermodynamics of Atmospheres & Oceans. *International*
421 *Geophysics Series*, 65, London: Academic Press.
422
- 423 Eckermann, S.D., Broutman, D., Ma, J., Doyle, J. D., Pautet, P. Taylor, M. J., et al. (2016).
424 Dynamics of Orographic Gravity Waves Observed in the Mesosphere over the Auckland Islands
425 during the Deep Propagating Gravity Wave Experiment (DEEPWAVE). *J. Atmos. Sci.*, *73*,
426 3855–3876. <https://doi.org/10.1175/JAS-D-16-0059.1>
427
- 428 Evensen, G. (1994). Sequential data assimilation with a nonlinear quasi-geostrophic model using
429 Monte Carlo methods to forecast error statistics. *J. Geophys. Res.*, *99*, 10 143–10 162.
430 <https://doi.org/10.1029/94JC00572>
431
- 432 Eyring, V., Arblaster, J. M., Cionni, I., Sedláček, J., Perlwitz, J., Young, P. J., et al. (2013).
433 Long-term ozone changes and associated climate impacts in CMIP5 simulations. *J. Geophys.*
434 *Res*, *118*, 5029-5060. <https://doi.org/10.1002/jgrd.50316>
435
- 436 Fang, T.-W., Anderson, D., Fuller-Rowell, T. J., Akmaev, R. Codrescu, M., Millward, G., et al.
437 (2013). Comparative studies of theoretical models in the equatorial ionosphere, in *Modeling the*
438 *Ionosphere-Thermosphere*, *Geophys. Monogr. Ser.*, *201*, edited by J. D.Huba, ISBN:978-0-
439 87590-491-7, 360 pp., AGU, Washington, D.C., USA
440
- 441 Feng, W., Marsh, D. R., Chipperfield, M. P., Janches, D., Höffner, J., Yi, F. et al. (2013). A
442 global atmospheric model of meteoric iron, *J. Geophys. Res. Atmos.*, *118*, 9456–9474.
443 <https://doi.org/10.1002/jgrd.50708>
444
- 445 Fomichev, V. I. & Blanchet J.-P. (1995). Development of the new CCC/GCM radiation model
446 for extension into the Middle Atmosphere, *Atmosphere-Ocean*, *33*, 513-529,
447 <https://doi.org/10.1080/07055900.1995.9649543>
448
- 449 Fomichev, V. I., Blanchet J.-P. & Turner D. S. (1998). Matrix parameterization of the 15 μm CO
450 2 band cooling in the middle and upper atmosphere for variable CO 2 concentration, *J. Geophys.*
451 *Res.*, *103*, 11505 – 11528, <https://doi.org/10.1029/98JD00799>
452
- 453 Fujiwara, H., & Miyoshi, Y. (2010). Morphological features and variations of temperature in the
454 upper thermosphere simulated by a whole atmosphere GCM, *Ann. Geophys.*, *28*, 427– 437,
455 <https://doi.org/10.5194/angeo-28-427-2010>
456

- 457 Fuller-Rowell, T. J., Akmaev, R. A., Wu, F., Anghel, A. F., Maruyama, N., Anderson, D. N., et
458 al (2008). Impact of terrestrial weather on the upper atmosphere, *Geophys. Res. Lett.*, *35*,
459 L09808, <https://doi.org/10.1029/2007GL032911>
460
- 461 Gardner, L. C., & Schunk, R. W., (2011), Large-scale gravity wave characteristics simulated
462 with a high-resolution global thermosphere-ionosphere model, *J. Geophys. Res.*, *116*, A06303,
463 <https://doi.org/10.1029/2010JA015629>
464
- 465 Gill, E., Sundaramoorthy, P., Bouwmeester, J., Zandbergen, B., & Reinhard, R. (2013).
466 Formation flying within a constellation of nano-satellites: The QB50 mission. *Acta Astronautica*,
467 *82*, 110-117. <https://doi.org/10.1016/j.actaastro.2012.04.029>
468
- 469 Goncharenko, L., Chau, J., Liu, H.-L., & Coster, A. J. (2010a). Unexpected connections between
470 the stratosphere and ionosphere. *Geophysical Research Letters*, *37*, L10101,
471 <https://doi.org/10.1029/2010GL043125>
472
- 473 Goncharenko, L., Coster, A. J., Chau, J., & Valladares, C. (2010b). Impact of sudden
474 stratospheric warmings on equatorial ionization anomaly. *Journal of Geophysical Research:*
475 *Space Physics*, *115*, A00G07,. <https://doi.org/10.1029/2010JA015400>
476
- 477 Griffin, D. J., and Thuburn, J. (2018). Numerical effects on vertical wave propagation in deep-
478 atmosphere models. *Quart. J. Roy. Met. Soc.*, *144*, 567-580
479
- 480 Heelis, R. A., Lowell, J. K., & Spiro, R. W. (1982). A Model of the High-Latitude Ionospheric
481 Convection Pattern, *J. Geophys. Res.* *87*, 6339-6345, <https://doi.org/10.1029/JA087iA08p06339>
482
- 483 Hsu, C. T., Matsuo, T., Wang, W., & Liu, J. Y. (2014). Effects of inferring unobserved
484 thermospheric and ionospheric state variables by using an Ensemble Kalman Filter on global
485 ionospheric specification and forecasting. *J. Geophys. Res. Space Physics*, *119*, 9256–9267,
486 <https://doi.org/10.1002/2014JA020390>
487
- 488 Immel, T.J., Sagawa, E., England, S.L., Henderson, S. B., Hagan, M. E., Mende, S. B., et al.
489 (2006). The control of equatorial ionospheric morphology by atmospheric tides. *Geophys. Res.*
490 *Lett.*, *33*, <https://doi.org/10.1029/2006GL026161>
491
- 492 Jin, H., Miyoshi, Y., Pancheva, D., Mukhtarov, P., Fujiwara, H., and Shinagawa, H. (2012).
493 Response of migrating tides to the stratospheric sudden warming in 2009 and their effects on the
494 ionosphere studied by a whole atmosphere-ionosphere model GAIA with COSMIC and
495 TIMED/SABER observations. *J. Geophys. Res.*, *117*, A10323,
496 <https://doi.org/10.1029/2012JA017650>
497
- 498 Kelly, C. W., Chipperfield, M. P., Plane, J.M. C., Feng, W., Sheese, P. E., Walker, K.A., et al.
499 (2018). An explanation for the nitrous oxide layer observed in the mesopause region.
500 *Geophysical Research Letters*, *45*, 7818-7827, <https://doi.org/10.1029/2018GL078895>
501

- 502 Knipp, D. J., Pette, D. V., Kilcommons, L. M., Isaacs, T. L., Cruz, A. A., Mlynczak, M. G. et
503 al. (2017). Thermospheric nitric oxide response to shock-led storms. *Space Weather*, *15*, 325–
504 342, <https://doi.org/10.1002/2016SW001567>
505
- 506 Lang, M., & Owens, M.J (2019). A Variational Approach to Data Assimilation in the Solar
507 Wind. *Space Weather*, *17*, 59-83. <https://doi.org/10.1029/2018SW0018>
508
- 509
- 510 Lejeune, S., Wautelet, G., & Warnant, R. (2012). Ionospheric effects on relative positioning
511 within a dense GPS network, *GPS Solutions*, *16* (1), 105–116, [https://doi.org/10.1007/s10291-](https://doi.org/10.1007/s10291-011-0212-1)
512 [011-0212-1](https://doi.org/10.1007/s10291-011-0212-1)
513
- 514 Lieberman, R. S., Akmaev, R. A., Fuller–Rowell, T. J., & Doornbos, E. (2013). Thermospheric
515 zonal mean winds and tides revealed by CHAMP. *Geophys. Res. Lett.*, *40*, 2439– 2443.
516 <https://doi.org/10.1002/grl.50481>
517
- 518 Liemohn, M., Ganushkina, N. Y., De Zeeuw, D. L., Rastaetter, L., Kuznetsova, M., Welling, D.
519 T., et al. (2018). Real-time SWMF at CCMC: Assessing the Dst output from continuous
520 operational simulations. *Space Weather*, *16*, 1583– 1603.
521 <https://doi.org/10.1029/2018SW001953>
522
- 523 Liu, H.-L., Bardeen, C. G., Foster, B. T., Lauritzen, P., Liu, J., Lu, G., et al. (2018).
524 Development and validation of the Whole Atmosphere Community Climate Model with
525 thermosphere and ionosphere extension (WACCM-X 2.0). *Journal of Advances in Modeling*
526 *Earth Systems*, *10*, 381–402. <https://doi.org/10.1002/2017MS001232>
527
- 528 Liu, H.-L., Foster, B. T., Hagan, M. E., McInerney, J. M., Maute, A., Qian, L., et al. (2010).
529 Thermosphere extension of the Whole Atmosphere Community Climate Model. *Journal of*
530 *Geophysical Research: Space Physics*, *115*, A12302. <https://doi.org/10.1029/2010JA015586>
531
- 532 Liu, H.-L., McInerney, J. M., Santos, S., Lauritzen, P. H., Taylor, M. A., & Pedatella, N. M.
533 (2014). Gravity waves simulated by high-resolution Whole Atmosphere Community Climate
534 Model. *Geophysical Research Letters*, *41*, 9106–9112. <https://doi.org/10.1002/2014GL062468>
535
- 536 Liu, H.-L., & Roble, R. G. (2002). A study of a self-generated stratospheric sudden warming and
537 its mesospheric–lower thermospheric impacts using the coupled TIME-GCM/CCM3. *Journal of*
538 *Geophysical Research: Atmospheres*, *107*(D23), 4695. <https://doi.org/10.1029/2001JD001533>
539
- 540 López-Valverde, M. A., and López-Puertas, M. (1994). A non-local thermodynamic equilibrium
541 radiative transfer model for infrared emissions in the atmosphere of Mars. 1: Theoretical basis
542 and nighttime populations of vibrational levels. *J. Geophys. Res.*, *99*, 13,093–13,115.
543 <https://doi.org/10.1029/94JE00635>.
544
- 545 Marsh, D. R., Garcia, R. R., Kinnison, D. E., Boville, B. A., Sassi, F., Solomon, S. C., et al.
546 (2007). Modeling the whole atmosphere response to solar cycle changes in radiative and
547 geomagnetic forcing. *J. Geophys. Res.*, *112*, D23306. <https://doi.org/10.1029/2006JD008306>.
548

- 549 Marsh, D.R, Mills, M. J., Kinnison, D. E., & Lamarque, J.-F.(2013). Climate Change from 1850
550 to 2005 Simulated in CESM1(WACCM). *J. Clim*, *26*, 7372-7391. <https://doi.org/10.1175/JCLI->
551 [D-12-00558.1](https://doi.org/10.1175/JCLI-D-12-00558.1)
552
- 553 Martynenko, O. V., Fomichev, V. I., Semeniuk, K., Beagley, S. R., Ward, W. E., McConnell,
554 J. C. et al. (2014). Physical mechanisms responsible for forming the 4-peak longitudinal
555 structure of the 135.6 nm ionospheric emission: First results from the Canadian IAM. *J.*
556 *Atmospheric and Solar-Terrestrial Physics*, *120*, 51-61.
557 <https://doi.org/10.1016/j.jastp.2014.08.014>
558
- 559 Maruyama, N., Sun, Y.-Y., Richards, P. G., Middlecoff, J., Fang, T.-W., Fuller-Rowell, T. J., et
560 al. (2016). A new source of the midlatitude ionospheric peak density structure revealed by a new
561 Ionosphere-Plasmasphere model. *Geophys. Res. Lett.*, *43*, 2429–2435.
562 <https://doi.org/10.1002/2015GL067312>
563
- 564 McCormack, J. P., Hoppel, K., Kuhl, D., de Wit, R., Stober, G., Espy, P., et al. (2017).
565 Comparison of mesospheric winds from a high-altitude meteorological analysis system and
566 meteor radar observations during the boreal winters of 2009–2010 and 2012–2013. *J. Atmos.*
567 *Sol.-Terr. Phys.*, *154*, 132–166. <https://doi.org/10.1016/j.jastp.2016.12.007>
568
- 569 McDonald, S. E., Sassi, F., Tate, J., McCormack, J., Kuhl, D. D., Drob, D. P., et al. (2018).
570 Impact of non-migrating tides on the low latitude ionosphere during a sudden stratospheric
571 warming event in January 2010. *Journal of Atmospheric and Solar-Terrestrial Physics*, *171*,
572 188-200. <https://doi.org/10.1016/j.jastp.2017.09.012>
573
- 574 Merlin, V. G., Kondrashov, D., Ghil, M., & Anderson, B. J. (2016). Data assimilation of low-
575 altitude magnetic perturbations into a global magnetosphere model. *Space Weather*, *14*, 165-
576 184. <https://doi.org/10.1002/2015SW001330>
577
- 578 Miyoshi, Y., Jin, H., Fujiwara, H., & Shinagawa, H. (2018). Numerical study of traveling
579 ionospheric disturbances generated by an upward propagating gravity wave. *J. Geophys. Res.:*
580 *Space Physics*, *123*, 2141– 2155. <https://doi.org/10.1002/2017JA025110>
581
- 582 Murray, S. A., Henley, E. M., Jackson, D. R. & Bruinsma, S. L. (2015). Assessing the
583 performance of thermospheric modeling with data assimilation throughout solar cycles 23 and
584 24. *Space Weather*, *13*, 220–232. <https://doi.org/10.1002/2015SW001163>.
585
- 586 Ogibalov V. P., & Fomichev, V. I., (2003). Parameterization of solar heating by the near IR CO2
587 bands in the mesosphere. *Adv. Space Res.*, *32*, 759-764. <https://doi.org/10.1016/S0273->
588 [1177\(03\)80069-8](https://doi.org/10.1016/S0273-1177(03)80069-8)
589
- 590 Pedatella, N. M., Liu, H.-L., Richmond, A. D., Maute, A., & Fang, T.-W. (2012). Simulations of
591 solar and lunar tidal variability in the mesosphere and lower thermosphere during sudden
592 stratosphere warmings and their influence on the low-latitude ionosphere. *Journal of Geophysi-*
593 *cal Research: Space Physics*, *117*, A08326. <https://doi.org/10.1029/2012JA017858>
594

- 595 Pedatella, N. M., Fang, T.-W., Jin, H., Sassi, F., Schmidt, H., Chau, J. L., et al. (2016).
596 Multimodel comparison of the ionosphere variability during the 2009 sudden stratosphere
597 warming. *J. Geophys. Res.*, *121*, 7204-7225. <https://doi.org/10.1002/2016JA022859>
598
- 599 Plane, J. M. C., Feng, W., & Dawkins, E. C. M. (2015). The Mesosphere and Metals: Chemistry
600 and Changes. *Chem Rev.*, *115*(10), 4497–4541. <https://doi.org/10.1021/cr500501m>
601
- 602 Scherliess, L., Tsagouri, I., Yizengaw, E., Bruinsma, S., Shim, J. S., Coster, A., & Retterer, J. M.
603 (2019). The International Community Coordinated Modeling Center space weather modeling
604 capabilities assessment: Overview of ionosphere/thermosphere activities. *Space Weather*, *17*,
605 527–538. [sunday morning coming down](https://doi.org/10.1002/2019SW002538)
606
- 607 Schunk, R. W., Scherliess, L., Eccles, V., Gardner, L. C., Sojka, J. J., Zhu, L., et al. (2016).
608 Space weather forecasting with a Multimodel Ensemble Prediction System (MEPS). *Radio Sci.*,
609 *51*, 1157– 1165. <https://doi.org/10.1002/2015RS005888>
610
- 611 Sheese, P. E., Walker, K. A., Boone, C. D., Bernath, P. F., and Funke, B. (2016), Nitrous oxide
612 in the atmosphere: First measurements of a lower thermospheric source, *Geophys. Res. Lett.*, *43*,
613 2866– 2872, doi:10.1002/2015GL067353.
614
- 615 Taylor, K.E., Stouffer, R. J., & Meehl, G. A. (2012). An Overview of CMIP5 and the
616 Experiment Design. *Bull. Amer. Meteor. Soc.*, *93*, 485–498, [https://doi.org/10.1175/BAMS-D-](https://doi.org/10.1175/BAMS-D-11-00094.1)
617 [11-00094.1](https://doi.org/10.1175/BAMS-D-11-00094.1)
618
- 619 Thuburn, J. (2008). Some conservation issues for the dynamical cores of NWP and climate
620 models. *J. Comput. Phys.*, *227*, 3715– 3730. <https://doi.org/10.1016/j.jcp.2006.08.016>
621
- 622 Ullrich, P. A., Jablonowski, C., Kent, J., Lauritzen, P. H., Nair, R., Reed, K. A., et al
623 (2017).DCMIP2016: a review of non-hydrostatic dynamical core design and intercomparison of
624 participating models. *Geosci. Model Dev.*, *10*, 4477-4509. [https://doi.org/10.5194/gmd-10-4477-](https://doi.org/10.5194/gmd-10-4477-2017)
625 [2017](https://doi.org/10.5194/gmd-10-4477-2017)
626
- 627 Vadas, S. L., and Fritts, D. C. (2005). Thermospheric responses to gravity waves: Influences of
628 increasing viscosity and thermal diffusivity. *J. Geophys. Res.*, *110*, D15103.
629 <https://doi.org/10.1029/2004JD005574>
630
- 631 Vadas, S. L., & Crowley, G. (2010). Sources of the traveling ionospheric disturbances observed
632 by the ionospheric TIDDBIT sounder near Wallops Island on October 30, 2007. *J. Geophys.*
633 *Res.*, *115*, A07324. <https://doi.org/10.1029/2009JA015053>
634
- 635 Wang, H., Akmaev, R. A., Fang, T.-W., Fuller-Rowell, T. J., Wu, F., Maruyama, N. et al.
636 (2014). First forecast of a sudden stratospheric warming with a coupled whole-
637 atmosphere/ionosphere model IDEA. *J. Geophys. Res. Space Physics*, *119*, 2079-2089.
638 <https://doi.org/10.1002/2013JA019481>
639

- 640 Weimer, D. (2005). Improved ionospheric electrodynamic models and application to calculating
641 Joule heating rates. *Journal of Geophysical Research*, *110*, A05306.
642 <https://doi.org/10.1029/2004JA010884>
643
- 644 Yiğit, E., Koucká Knížová, P., Georgieva, K. & Ward, W. (2016). A review of vertical coupling
645 in the Atmosphere–Ionosphere system: Effects of waves, sudden stratospheric warmings, space
646 weather, and of solar activity. *Journal of Atmospheric and Solar-Terrestrial Physics*, *141*, 1-12.
647 <https://doi.org/10.1016/j.jastp.2016.02.011>
648
- 649 Yiğit, E., Aylward, A. D., & Medvedev, A. S., (2008). Parameterization of the effects of
650 vertically propagating gravity waves for thermosphere general circulation models: Sensitivity
651 study. *J. Geophys. Res.*, *113*, D19106. <https://doi.org/10.1029/2008JD010135>

